Journal of Power Sources 231 (2013) 197–202

Contents lists available at SciVerse ScienceDirect

Journal of Power Sources

journal homepage: www.elsevier.com/locate/jpowsour

Highly ordered mesoporous phenol–formaldehyde carbon as supercapacitor electrode material

Tingwei Cai, Min Zhou, Dayong Ren, Guangshuai Han, Shiyou Guan*

School of Materials Science and Engineering, East China University of Science and Technology, Mei Long Road 130, Shanghai 200237, PR China

HIGHLIGHTS

- The C-FDU-16 was synthesized and modified by nitric acid treatment.
- The N-FDU-16 with acid-modification possesses good supercapacitive properties.
- The N-FDU-16 exhibits 7 times larger capacitance than the C-FDU-16.
- The N-FDU-16 shows excellent cycling stability after 10000 cycles.

ARTICLE INFO

Article history:
Received 31 August 2012
Received in revised form
27 October 2012
Accepted 17 December 2012
Available online 24 December 2012

Keywords:
Ordered mesoporous carbon
Phenol–formaldehyde carbon
Chemical modification
Specific capacitance
Supercapacitor

ABSTRACT

Highly ordered, body-centered cubic mesoporous phenol–formaldehyde carbon C-FDU-16 is prepared by a facile evaporation induced self-assembly strategy under a basic aqueous condition. Afterwards, in order to increase the active site of surface electrochemical reactions and promote the wettability in aqueous electrolyte, a simple chemical surface modification is carried out on the C-FDU-16 by nitric acid treatment. The C-FDU-16 and the acid-modified C-FDU-16 (N-FDU-16) are used as the active materials for supercapacitors. Although C-FDU-16 has unique 3D mesoporous network combined with high specific surface area, it do not show well supercapacitor properties for its bad wettability with the aqueous electrolyte. However, the N-FDU-16 with acid treatment exhibits the largest specific capacitance of 219 F g^{-1} at a current density of 0.1 A g^{-1} in 1 M H_2SO_4 electrolyte which is 7 times larger than that of the C-FDU-16 and it also shows good cycling stability as well. Therefore, based on the above investigations, ordered mesoporous phenol–formaldehyde carbon such as C-FDU-16 can be a potential candidate for supercapacitors after the simply acid treatment.

1. Introduction

In response to the need of modern society and emerging ecological, the development of new electrochemical energy storage/convert systems with high-performance, low-cost and environmentally friendly is more and more essential [1,2]. Supercapacitors, as an ideal energy storage system, are not limited by the electrochemical charge transfer kinetics of batteries and thus can operate at very high charge and discharge rate [3–5]. They can be charged and discharged for hundreds of thousands cycles without adversely affecting their lifetime; it is known that batteries suffer from a low cycling life (generally < 1000).

Usually, the supercapacitors can be classified as faradaic pseudocapacitors and electrical double-layer capacitors (EDLCs) based on the principle of energy storage [3]. As we know, the supercapacitor electrode materials of faradaic pseudocapacitors are commonly transition metal oxides [3,6] and conducting polymers [7,8]. Meanwhile, carbon materials are commonly used in EDLCs [9–14]. The faradaic pseudocapacitors exhibit higher capacitance than that of EDLCs, but the phase changes in the pseudocapacitance materials, low surface area and poor electrical conductivity limit their lifetime and power density. Carbon, in its various forms, has been used as the most ideal materials for supercapacitors, aiming at high specific capacitance together with high power density. At present, high-surface-area activated carbons (ACs) are still the predominant electrode materials for commercial supercapacitors. However, for ACs typically only about 10–20% of the "theoretical" capacitance was observed due to the presence of micropores that are inaccessible by the electrolyte, wetting deficiencies of electrolytes on the electrode surface, and/or the inability to successfully form a double layer in pores [15,16]. Meanwhile, the broad distribution of pore size, significantly decreases the specific capacitance of ACs.

* Corresponding author. Tel./fax: +86 21 64251509.
E-mail address: syguan@ecust.edu.cn (S. Guan).

0378-7753/$ – see front matter © 2012 Elsevier B.V. All rights reserved.
http://dx.doi.org/10.1016/j.jpowsour.2012.12.072

Ordered mesoporous carbons (OMCs) which possess large surface area, uniform pore size, specific channels and structural regularity, seem to be attractive candidates as electrode materials for supercapacitors.

Up to now, various methods such as soft template replicating, hard template nanocasting and self-assembly have been successfully employed to prepare OMCs with different porous structures [16–20]. Among them, a kind of ordered two-dimensional (2D) hexagonally mesoporous carbon as CMK-3, and ordered 3D cubic mesoporous carbon as CMK-1 and CMK-8 have been widely investigated as electrode materials for EDLCs [21–23]. Both of them are prepared via a direct-templating nanocasting using ordered mesoporous silica SBA-15 and KIT-6, respectively. Mesoporous carbon replicas can be obtained through the following procedures: irrigating the precursor such as sucrose into the silica channels, hydrothermal at a certain temperature, and removing the hard templates by using HF or NaOH solution. It is an obviously multistep preparation procedure and timing-consuming, and sacrifices both templates, thus fussy and expensive.

Recent years, a new kind of highly ordered mesoporous resin/carbon has been developed by an evaporation induced self-assembly strategy with low-molecular-weight phenolic resin precursors (resols) and triblock copolymer templates [24–26]. Compared with nanocasting mesoporous carbon and ACs, ordered mesoporous phenol–formaldehyde carbons do not only have fascinating essential application in supercapacitors as electrode materials, but also may be produced in industry for its low-cost and simple fabrication process.

Herein, ordered mesoporous carbon C-FDU-16 with 3D body-centered cubic mesostructured channels was prepared through an evaporation induced self-assembly strategy using F127 as template [25,26]. The unique 3D network of C-FDU-16 could facilitate ion diffusion throughout the nanochannels without pore blockage, which probably makes the surface of C-FDU-16 favorable for charging the electric double-layer [27]. Also, in order to increase oxygen-containing functional groups on the pore surface of the C-FDU-16 and promote its wettability in aqueous electrolyte, the C-FDU-16 was surface modified by treatment with nitric acid [28,29]. The supercapacitive properties of the unmodified and acid-modified C-FDU-16 were first studied in this paper. The results showed that C-FDU-16 has poor supercapacitive properties, but it was obviously improved by acid modification.

2. Experimental

Triblock copolymer Pluronic F127 ($M_w = 12600$, $EO_{106}PO_{70}EO_{106}$) were purchased from Aldrich Chemical Inc. Other chemicals were purchased from Shanghai Chemical Corp. All chemicals were used as received without any further purification. Deionized water was used in all experiments.

2.1. Synthesis of phenol–formaldehyde mesoporous carbon C-FDU-16

Mesoporous carbon material C-FDU-16 was synthesized by using triblock copolymer as a template and phenol/formaldehyde as carbon precursor according to the literature [25,26].

2.1.1. Resol precursor preparation

A soluble low-molecular-weight polymer ($M_w = \sim 500$) derived from resol was prepared by basic polymerization. Typically, 6.1 g (65.0 mmol) phenol was melted at 40–42 °C before 20% NaOH (aq: 1.3 g, 6.5 mmol) was added slowly over 10 min with stirring. Formalin (37 wt.%, 10.5 g) containing formaldehyde (130.0 mmol) was added dropwise, and the reaction mixture was stirred at 70 °C for 1 h. After cooling the mixture to room temperature, the pH of the reaction mixture was adjusted to neutral (7.0) using 0.6 M HCl solution. Water was then removed under vacuum below 50 °C. The final product ($M_w < 500$ measured by GPC) was redissolved in ethanol (63.6 g) and the salt NaCl was filtered before use.

2.1.2. Synthesis of mesoporous polymer FDU-16

Triblock copolymer poly(ethylene oxide)-b-poly(propylene oxide)-b-poly (ethylene oxide) (PEO-PPO-PEO, pluronic 127: 0.3 g) was dissolved in ethanol (4.5 g), then the ethanol solution of the above precursors (5.07 g) containing phenol (0.4 g, 4.3 mmol) and (0.26 g, 8.6 mmol) formaldehyde was added by stirring for 10 min to form a homogeneous solution. The solution was transferred to a dish and the ethanol evaporated at room temperature over 8 h and then heated in an oven at 120 °C for 24 h to thermopolymerize the phenolic resins. The products were calcined at 350 °C under nitrogen for 5 h with a temperature increase rate of 1 °C min^{-1} to obtain the porosity and decomposition of the amphiphilic triblock copolymer template.

2.1.3. Carbonization of FDU-16

Mesoporous carbon material C-FDU-16 was prepared by direct transformation of the corresponding mesostructured polymer by carbonization under nitrogen. Carbonization was carried out in a tube oven under nitrogen at 800 °C for 2 h. The temperature was increased at a rate of 1 °C min^{-1} and held at 200, 350, 500 °C for 2 h before reaching the final temperature.

2.2. Chemical modification of C-FDU-16

The C-FUD-16 carbon was chemically modified using HNO_3 solution. Briefly, 0.1 g of C-FDU-16 was suspended in 10 mL of concentrated HNO_3 (68 wt.%) and then refluxed at 65 °C for 1 h. After the mixture was cooled down to room temperature, it was filtered and washed with deionized water until the pH value of the filtrate was around 7. Then the product was dried at 80 °C for 12 h in air. The nitric-acid-modified C-FDU-16 carbon was denoted as N-FDU-16.

2.3. Structural characterization

Transmission electron microscopy (TEM) measurements were conducted on a JEM-2100 transmission electron microscope (JEOL, Japan). The Brunauer–Emmett–Teller (BET) method was used to determine the surface area by measuring the adsorption of N_2 at 77 K using a NOVA 4200e (Quantachrome, USA) instrument. Before measurement, the sample was degassed at a temperature of 180 °C for 8 h. Powder X-ray diffraction (XRD) pattern was obtained on a D/MAX 2550 VB PC^{-1} diffractometer (Rigaku, Japan) using Cu Kα radiation ($\lambda = 0.154$ nm). The chemical composition of the samples were analyzed by Fourier transformation infrared spectroscopy (FTIR) using a Nicolet 5700 (Thermo Electron Crop., USA). The surface functionality of the N-FDU-16 was analyzed on Perkin–Elmer PHI-5000C multifunctional X-ray photoelectron spectroscope (XPS, physical Electronics, USA).

2.4. Electrode preparation and electrochemical measurements

To prepare the working electrode, the as-made mesoporous carbon materials were ground with acetylene black (10 wt.%), and polytetrafluoroethylene (PTFE, 10 wt.%) and then pressed onto titanium gauze at 5 MPa. The electrode assembly was dried for 12 h at 80 °C in air. Each carbon electrode contained about 6 mg of electroactive material and had a geometric surface area about 1 cm^2. The capacity was calculated with respect to mesoporous carbon.

Electrical measurements were performed with an electrochemical analyzer, CHI 660D (Shanghai Chenhua Limited Co.) under ambient conditions in 1 M H_2SO_4 aqueous solution, using a three-electrode system, with the mesoporous carbon as the working electrode, a platinum wire as the counter electrode and an Ag/AgCl electrode (3 M KCl solution) as the reference electrode.

The cyclic voltammetry (CV) measurements were conducted with a potential window from −0.1 V to 0.7 V at different scan rate ranging from 1 mV s^{-1} to 50 mV s^{-1}. Galvanostatic charge/discharge measurements were run on from −0.1 V to 0.7 V at different current densities. Electrochemical impedance spectroscopy (EIS) measurements were recorded from 100 KHz to 10 mHz with an alternate current amplitude of 5 mV. Capacitance values were calculated from the slopes of the discharge curves by the formula:

$$C = \frac{I \times \Delta t}{\Delta E \times m} \quad (1)$$

where C is the specific capacitance, I is the constant discharging current, Δt is the discharging time, ΔE is the discharging potential window and m is the mass of the corresponding electrode material.

3. Results and discussion

3.1. Microstructure characterizations

The microstructures of the C-FDU-16 and the N-FDU-16 carbon were examined by TEM. Fig. 1a shows TEM images shows that C-FDU-16 exhibits a well-ordered mesostructure in the whole domain. Moreover, the N-FDU-16 shown in Fig. 1b has exactly the same TEM morphology as the C-FDU-16, which indicates that the acid-modification did not destroy the intrinsic ordered cubic (*Im3m*) mesostructure.

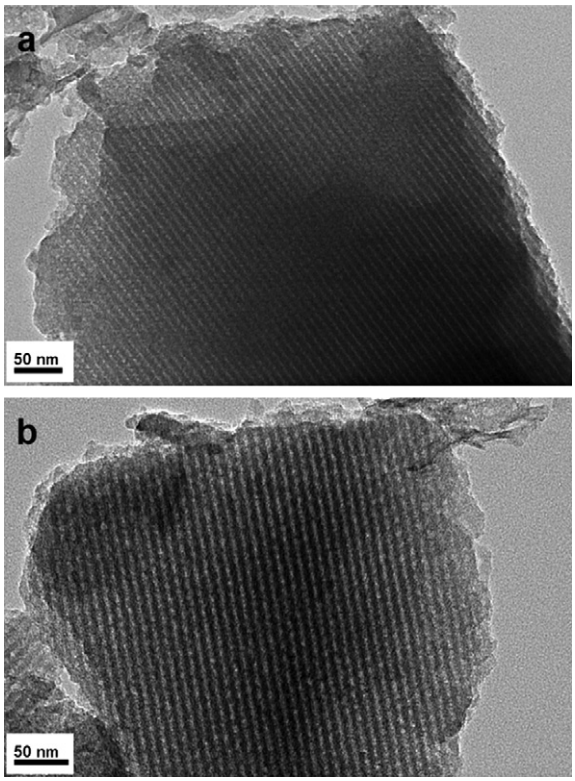

Fig. 1. TEM images of (a) the C-FDU-16 and (b) the N-FDU-16.

Small-angle XRD patterns of the C-FDU-16 and the N-FDU-16 are shown in Fig. 2. Both the samples show a strong peak at around 0.9°, which is indexed as (1 1 0) diffraction of the 3D cubic *Im3m* symmetry [25]. Moreover, compared with C-FDU-16, there is no obvious change in intensity and position of the peak for N-FDU-16. It further confirms that the ordered mesoporous structure can be well preserved and the pore-size did not take place obvious change after acid-modification.

The FTIR spectra of C-FDU-16 carbon before and after acid-modification are shown in Fig. 3. The major features of the spectra of these carbons are similar with bands at 1128 cm^{-1} and a broad band at around 3432 cm^{-1} which is mainly caused by the O—H stretching vibration of the absorbed water molecules. The band at 1128 cm^{-1} is caused by the stretching vibration of the C—O bonds. In addition, the C═O stretching vibrations related to carbonyl and/or carboxyl groups can be found at around 1730 cm^{-1}. Compared with C-FDU-16, a new band at 1260 cm^{-1} which can be assigned tentatively to C—O—C vibrations in ether structures or other single bonded oxo group C—O—R is found [28]. The acid modification of the C-FDU-16 can significantly affect the surface functionality.

From XPS test, it is confirmed that O (14.77 at.%) and N (0.82 at.%) were introduced during acid treatment, and oxygen-containing C groups (including C—OR, C═O and —O—C═O) were formed. The chemical nature of these functional groups was determined by deconvolution of the C_{1s} peak. As shown in Fig. 4, deconvolution of C_{1s} spectrum gives five peaks representing carbon atoms bonded to carbon, nitrogen and oxygen atoms. These five peaks are related to C—C bond (284.4 eV), C—N bond (285.6 eV), C—OR (286.4 eV), C═O (287.3 eV) and —O—C═O (288.6 eV), respectively. The C—N, C—O, C═O and —O—C═O fractions are as high as 13.55 at.%, 8.29 at.%, 8.67 at.% and 3.94 at.% in N-FDU-16, respectively, indicating a significant amount of N— and O— containing groups. In fact, these functional groups on such as C—N group and pyrone-like functionalities (part of C═O and C—O) in the surface of nanochannels of the N-FDU-16 carbon can make effects on the wettability in aqueous electrolyte and electrochemical capacitive behaviors [30,31].

The specific surface area and pore-size distribution analyses of the C-FDU-16 and the N-FDU-16 samples were conducted using N_2 adsorption and desorption experiments. Both of the two samples show typical type IV curves with a H_2-type hysteresis loop (Fig. 5),

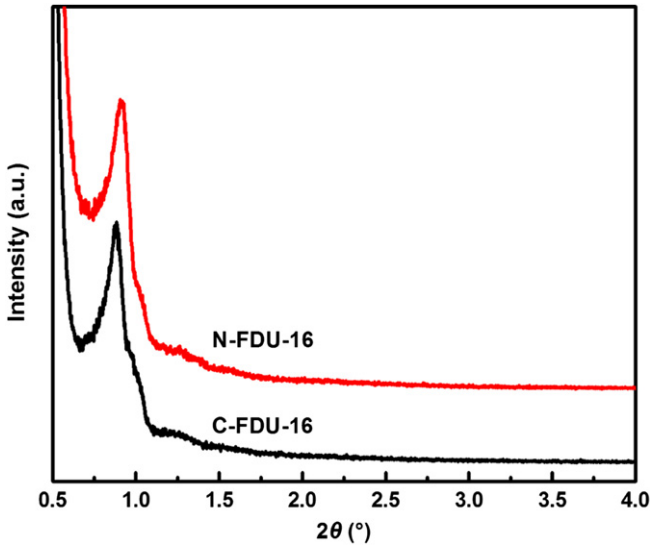

Fig. 2. The small-angle XRD patterns of the C-FDU-16 and the N-FDU-16.

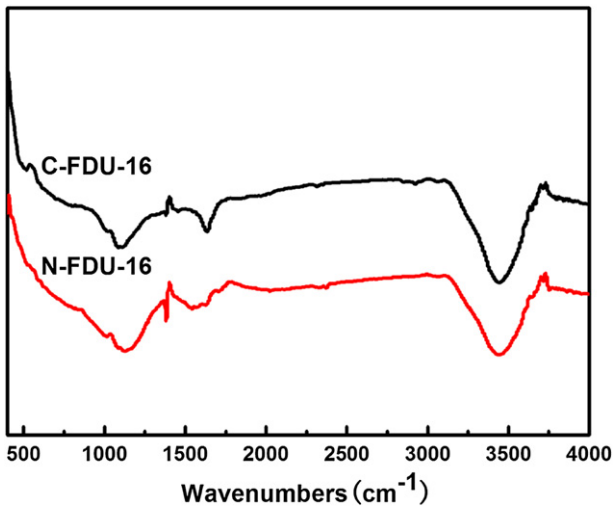

Fig. 3. The FTIR of spectra of the C-FDU-16 and the N-FDU-16.

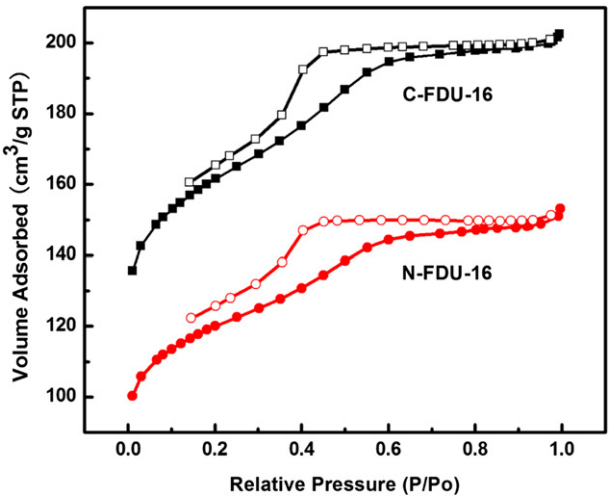

Fig. 5. N_2 adsorption–desorption isotherms of the C-FDU-16 and the N-FDU-16.

implying a cage-like mesopore. The pore size distribution curve is narrow at mean value around 2.2 nm, clearly indicating that the mesoporous carbons have a well-defined uniform pore size before and after acid-modification. In detail, the BET surface area of the C-FDU-16 is 548 $m^2\ g^{-1}$, the mesopore volume is 0.31 $cm^3\ g^{-1}$, and the average pore diameter is 2.3 nm. The BET surface area of the N-FDU-16 is 408 $m^2\ g^{-1}$, its mesoporous volume is 0.24 $cm^3\ g^{-1}$, and the average pore diameter is 2.3 nm. The slight decrease in the specific surface area and pore volume could be ascribed to the functional groups (including C—OR, C═O and —O—C═O) introduced by acid-treatment on the pore walls, which will occupy some space of the pores and decrease the uptake of N_2 during the BET test [28].

3.2. Electrochemical test

CV and galvanostatic charge/discharge measurements were employed to evaluate the electrochemical properties and to calculate the specific capacitances of the as-prepared C-FDU-16 and N-FDU-16 electrodes. Fig. 6a shows the CV curves of the C-FDU-16 and N-FDU-16 electrodes at the scan rate of 1 mV s^{-1} between −0.1 V and 0.7 V (vs. Ag/AgCl) in 1 M H_2SO_4 aqueous electrolyte. It can be seen that the shape of the C-FDU-16 electrode is obviously different from the EDLCs' typical rectangular shape, which indicates the C-FDU-16 without any treatment has poor electrochemical properties when it is used as a supercapacitor electrode. Nevertheless, the CV curve of the N-FDU-16 electrode deviated from idealized double-layer behaviors with a pair of broad, superimposed and reversible faradaic surface redox reactions, behaving as pseudocapacitance. It was attributed to redox reactions of the O functionalities on the surface of the N-FDU-16 [30,31]. Moreover, it is clear that the N-FDU-16 electrode exhibits a much higher specific capacitance compared with the untreated C-FDU-16. It's mainly because that the oxygenated groups on the surface not only provide pseudo-capacitance but also improve the wettability of the electrode in aqueous electrolyte notably [29]. The specific capacitance values for the C-FDU-16 and N-FDU-16 electrodes which obtained from the CV curves in Fig. 6a are 37 and 139 F g^{-1}, respectively.

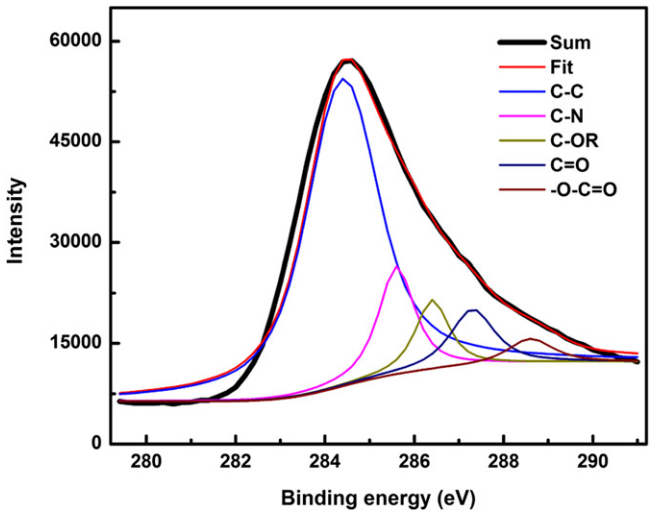

Fig. 4. C_{1s} XPS spectra of the N-FDU-16.

Fig. 6b shows the CV curves of the N-FDU-16 electrode at different scan rates. No obvious distortion in the CV curves to be observed as the sweep rate increased in the range of 1 mV s^{-1} to 20 mV s^{-1} which suggesting a highly reversible system in the H_2SO_4 electrolyte within the potential range employed. However, the distortion becomes sharp when the scan rate reaches to 50 mV s^{-1}, which reflecting a more significant ohmic resistance in pores.

The charge/discharge curves of the C-FDU-16 and N-FDU-16 electrodes within a potential window of −0.1 V to 0.7 V at a current density of 0.1 A g^{-1} are shown in Fig. 7a and the charge/discharge curves of the N-FDU-16 electrode at different current densities are shown in Fig. 7b. It is clear seen that the shape of the charge/discharge curves of these two electrodes are closely linear and show a typical triangle symmetrical distribution, indicating a good double layer capacitive property. Nevertheless, the charge/discharge time in one cycle of the N-FDU-16 electrode is much longer than that of the C-FDU-16 electrode, which directly indicates an obvious improvement in capacitance properties by acid-modification. The specific capacitance values for the C-FDU-16 and N-FDU-16 electrodes obtained from the charge/discharge curves in Fig. 7a according to formula (1) were 32 (0.1 A g^{-1}) and 219 F g^{-1} (0.1 A g^{-1}), respectively.

To further understand the high rate capability of the C-FDU-16 and N-FDU-16 electrodes, the charge/discharge measurements were recorded at different current densities. Fig. 7c reveals that the values of the specific capacitance for both the two electrodes are

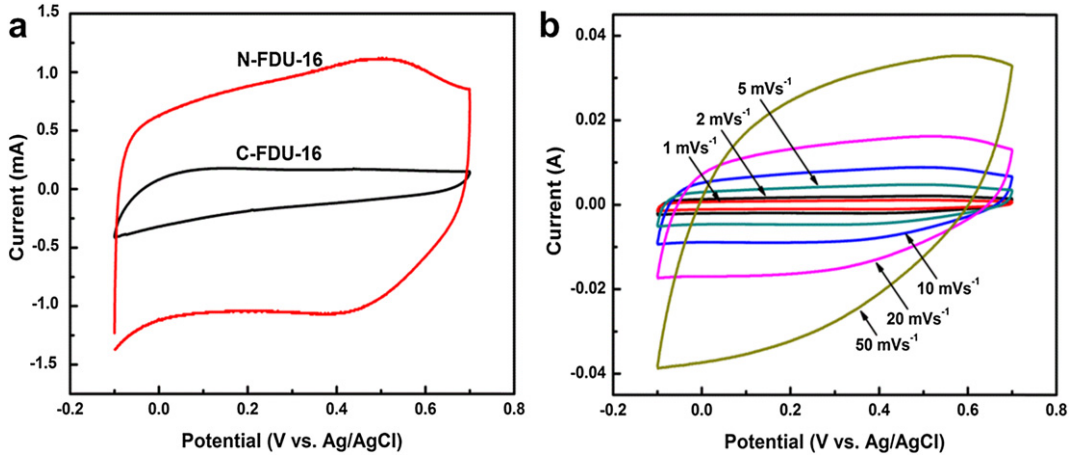

Fig. 6. CV curves of (a) the C-FDU-16 and N-FDU-16 electrodes at sweep rate of 1 mV s^{-1} and (b) the N-FDU-16 electrode at different sweep rates.

strongly dependent on the current densities. In detail, the specific capacitance severely decreases with the increase of the current density below 1 A g^{-1}, but it becomes slightly high at large current densities. Compared with the C-FDU-16 electrode, the N-FDU-16 electrode not only exhibits much larger specific capacitance at a small current density, but also can remain an ideal specific capacitance of 108 F g^{-1} at a high charge/discharge current density of 5 A g^{-1}. It indicates that the high rate capability of the C-FDU-16 can be preserved after surface acid treatment. The results also show that the N-FDU-16 electrode allow rapid ion diffusion and exhibit good electrochemical utilization rather than the C-FDU-16. Here, the unique 3D mesoporous network can facilitate ion transport throughout the pore channels without pore blockage, which makes the surface of N-FDU-16 with improved wettability in aqueous favorable for charging the electric double-layer and ions diffusion.

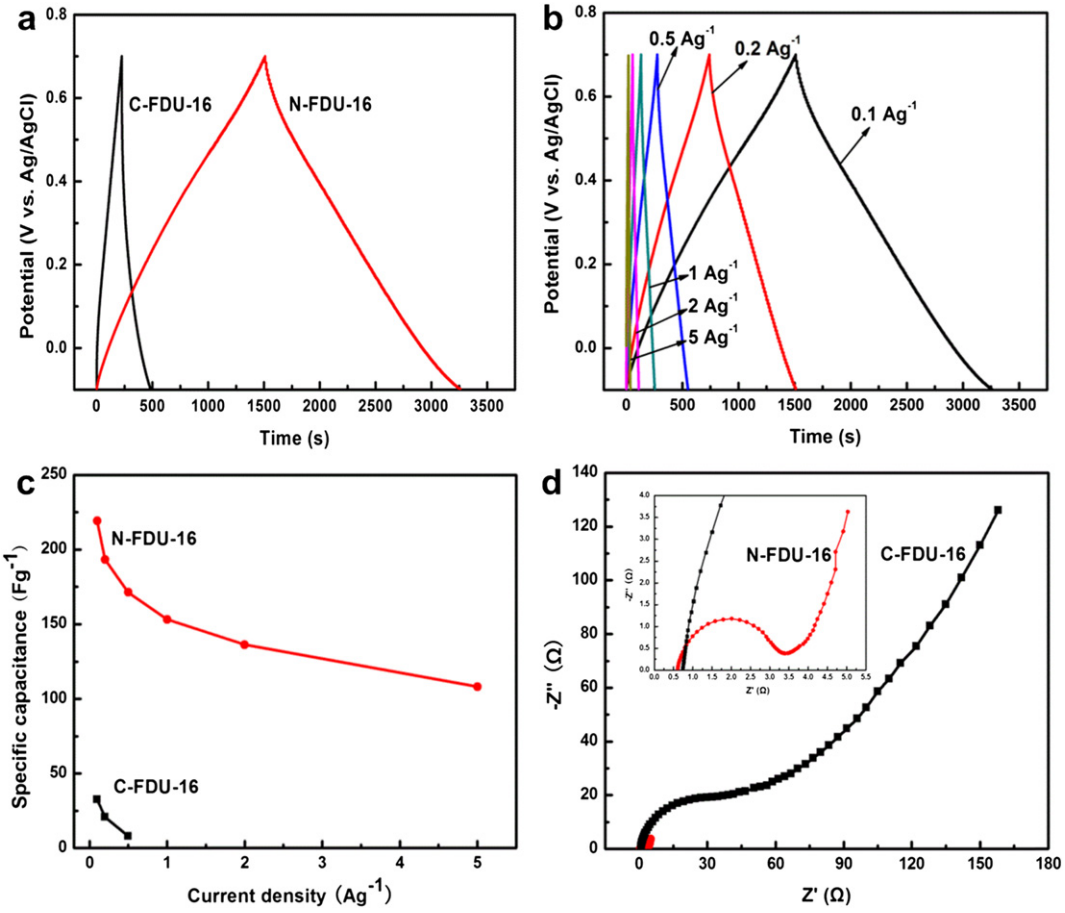

Fig. 7. The charge–discharge curves of (a) the C-FDU-16 and N-FDU-16 electrodes at a current density of 0.1 A g^{-1} and (b) the N-FDU-16 electrode at different current densities; (c) The specific capacitance of the C-FDU-16 and N-FDU-16 electrodes at different current densities; (d) Complex–plane impedance plots of the C-FDU-16 and N-FDU-16 electrodes. The inset is the high frequency regions.

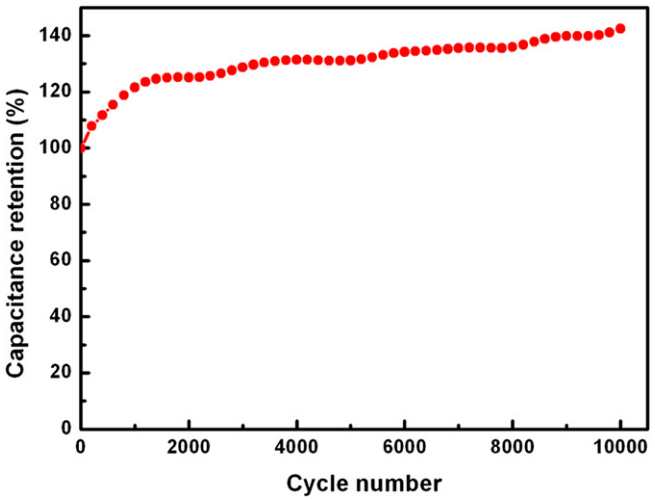

Fig. 8. Cycle stability of the N-FDU-16 electrode at the current density of 1 A g^{-1} in 1 M H_2SO_4 electrolyte.

The complex plane plots of the AC impedance spectra for the C-FDU-16 and N-FDU-16 were shown in Fig. 7d. It is seen that the plots both exhibit two distinct traits: a semicircle in the high frequency range and a sloped line in the low frequency range. From the point intersecting with the real axis in the range of high frequency, the internal resistance of the electrode material includes the total resistance of the ionic resistance of the electrolyte, the intrinsic resistance of active material, and the contact resistance at the active material/current collector interface. The semicircle in the high-frequency range associates with the surface properties of the porous electrode, which corresponds to the faradic charge transfer resistance. At the lower frequencies, a straight sloping line represents the diffusive resistance of the electrolyte in electrode pores and the proton diffusion in host material. It should be mentioned that the two carbon electrodes have the same small internal resistance. Nevertheless, there is obvious difference between the two spectra. The semicircle of the N-FDU-16 is much smaller than that of the C-FDU-16, indicating lower charge transfer resistance. Moreover, the N-FDU-16 has a larger Warburg angle than that of the C-FDU-16, suggesting faster electrolyte diffusion in the N-FDU-16 electrode pores.

Long cycling life is an important requirement for supercapacitor electrodes. The cycle stability of the N-FDU-16 electrode was evaluated at the current density of 1 A g^{-1} between −0.1 V and 0.7 V for 10000 cycles. The capacitance retention ratio as a function of cycle number is displayed in Fig. 8. According to the literature [32,33], the activation of electroactive material only takes place in the first hundreds cycles. But, for the N-FDU-16, this process is still progressing until and over 10000 cycles because the 3D mesoporous network structure of the electroactive material slows down the diffusion of electrolyte to the inner pores. As the result, the capacitance of the N-FDU-16 is constantly increased. After 10000 continuous cycles, the N-FDU-16 electrode finally displays excellent long cycle life for the improved wettability of the electrode and the long-term electrochemical stability, which is significant for the practical application.

4. Conclusions

In summary, the ordered body-centered cubic mesoporous phenol–formaldehyde carbon C-FDU-16 was synthesized by a facile evaporation induced self-assembly strategy and its surface chemical modification was employed by nitric acid treatment. The C-FDU-16 electrode shows poor supercapacitive properties for its terrible wettability in aqueous electrolyte. Nevertheless, the carbon with acid-modification N-FDU-16 possesses good supercapacitive properties due to the improved surface with oxygenated groups which introduce large pseudocapacitance and enhance the wettability in aqueous electrolyte. As a result, the interconnected 3D mesoporous network of phenol–formaldehyde carbon can facilitate ion diffusion throughout the pore channels without pore blockage. The N-FDU-16 electrode with acid treatment shows the largest specific capacitance of 219 F g^{-1} at 0.1 A g^{-1} which is 7 times larger than that of C-FDU-16 without acid-modification. Moreover, the N-FDU-16 electrode exhibits excellent cycling stability and lifetime. These encouraging results illustrate the exciting potential for the low-cost ordered mesoporous phenol–formaldehyde carbon used in high performance supercapacitors with simply acid treatment.

References

[1] M. Winter, R.J. Brodd, Chem. Rev. 104 (2004) 4245–4269.
[2] S.L. Xiong, C.Z. Yuan, X.G. Zhang, B.J. Xi, Y.T. Qian, Chem. Eur. J. 15 (2009) 5320–5326.
[3] B.E. Conway, Electrochemical Supercapacitors Scientific Fundamentals and Technological Applications, Kluwer Academic/Plenum Publishers, New York, 1999.
[4] Z.S. Wu, D.W. Wang, W.C. Ren, J.P. Zhao, G.M. Zhou, F. Li, H.M. Cheng, Adv. Funct. Mater. 20 (2010) 3595–3602.
[5] J.W. Lang, L.B. Kong, W.J. Wu, Y.C. Luo, L. Kang, Chem. Commun. 35 (2008) 4213–4215.
[6] S. Boukhalfa, K. Evanoff, G. Yushin, Energy Environ. Sci. 5 (2012) 6872–6879.
[7] P. Sivaraman, S.P. Mishra, A.R. Bhattacharrya, A. Thakur, K. Shashidhara, A.B. Samui, Electrochim. Acta 69 (2012) 134–138.
[8] H.H. Chang, C.K. Chang, Y.C. Tsai, C.S. Liao, Carbon 50 (2012) 2331–2336.
[9] G.H. Sun, J. Wang, K.X. Li, Y.Q. Li, L.J. Xie, Electrochim. Acta 59 (2012) 424–428.
[10] P. Kossyrev, J. Power Sources 201 (2012) 347–352.
[11] S.J. Han, Y.H. Kim, K.S. Kim, S.J. Park, Curr. Appl. Phys. 12 (2012) 1039–1044.
[12] K. Xie, X.T. Qin, X.Z. Wang, Y.N. Wang, H.S. Tao, Q. Wu, L.J. Yang, Z. Hu, Adv. Mater. 24 (2012) 347–352.
[13] H.M. Sun, L.Y. Cao, L.H. Lu, Energy Environ. Sci. 5 (2012) 6206–6213.
[14] C.W. Huang, C.T. Hsieh, P.L. Kuo, H.S. Teng, J. Mater. Chem. 22 (2012) 7314–7322.
[15] M. Anouti, L. Timperman, M. hilali, A. Boisset, H. Galiano, J. Phys. Chem. C 116 (2012) 9412–9418.
[16] H.L. Lu, W.J. Dai, M.B. Zheng, N.W. Li, G.B. Ji, J.M. Cao, J. Power Sources 209 (2012) 243–250.
[17] W. Xing, S.Z. Qiao, R.G. Ding, F. Li, G.Q. Lu, Z.F. Yan, H.M. Cheng, Carbon 44 (2006) 216–224.
[18] D.W. Wang, F. Li, M. Liu, G.Q. Lu, H.M. Cheng, Angew. Chem. Int. Ed. 47 (2008) 373–376.
[19] M. Li, J.M. Xue, J. Colloid Interface Sci. 377 (2012) 169–175.
[20] Y.K. Lv, L.H. Gan, M.X. Liu, W. Xiong, Z.J. Xu, D.Z. Zhu, D.S. Wright, J. Power Sources 209 (2012) 152–157.
[21] K.S. Xia, Q.M. Gao, J.H. Jiang, J. Hu, Carbon 46 (2008) 1718–1726.
[22] J.W. Lang, X.B. Yan, X.Y. Yuan, J. Yang, Q.J. Xue, J. Power Sources 196 (2011) 10472–10478.
[23] J.W. Lang, X.B. Yan, W.W. Liu, R.T. Wang, Q.J. Xue, J. Power Sources 204 (2012) 220–229.
[24] Y. Meng, D. Gu, F.Q. Zhang, Y.F. Shi, H.F. Yang, Z. Li, C.Z. Yu, B. Tu, D.Y. Zhao, Angew. Chem. Int. Ed. 44 (2005) 7053–7059.
[25] Y. Meng, D. Gu, F.Q. Zhang, Y.F. Shi, L. Cheng, D. Feng, Z.X. Wu, Z.X. Chen, Y. Wan, A. Stein, D.Y. Zhao, Chem. Mater. 18 (2006) 4447–4464.
[26] Y. Huang, H.Q. Cai, T. Yu, F.Q. Zhang, F. Zhang, Y. Meng, D. Gu, Y. Wan, X.L. Sun, B. Tu, D.Y. Zhao, Angew. Chem. Int. Ed. 46 (2007) 1089–1093.
[27] M. Oschatz, E. Kockrick, M. Rose, L. Borchardt, N. Klein, I. Senkovska, T. Freudenberg, Y. Korenblit, G. Yushin, S. Kaskel, Carbon 48 (2010) 3987–3992.
[28] P.A. Bazula, A.H. Lu, J.J. Nitz, F. Schüth, Microporous Mesoporous Mater. 108 (2008) 266–275.
[29] F. Lufrano, P. Staiti, Energy Fuels 24 (2010) 3313–3320.
[30] M.P. Bichat, E. Raymundo-Piñero, F. Béguin, Carbon 48 (2010) 4351–4361.
[31] V. Khomenko, E. Raymundo-Piñero, F. Béguin, J. Power Sources 195 (2010) 4234–4241.
[32] H. Wang, Q. Hao, X. Yang, L. Lu, X. Wang, Nanoscale 2 (2010) 2164–2170.
[33] C.Z. Yuan, X.G. Zhang, L.H. Su, B. Gao, L.F. Shen, J. Mater. Chem. 19 (2009) 5772–5777.